Thermodynamics and Kinetics of Glyoxal Dimer Formation: A Computational Study

Jeremy Kua,* Sean W. Hanley, and David O. De Haan

Department of Chemistry, University of San Diego, 5998 Alcala Park, San Diego, California 92110

Received: August 15, 2007; In Final Form: October 11, 2007

Density functional theory (B3LYP//6-311+G*) calculations including Poisson−Boltzmann implicit solvent were used to study the hydration of glyoxal and subsequent formation of dimeric species in solution. Our calculations show that the dioxolane ring dimer is the thermodynamic sink among all monomers and dimers with varying degrees of hydration. Although fully hydrated species are thermodynamically favored over their less hydrated counterparts, we find that a preliminary dehydration step precedes dimerization and ring closure. Ring closure of the open dimer monohydrate to the dioxolane ring dimer is kinetically favored over both hydration to the open dimer dihydrate and ring closure to form the dioxane ring dimer. The kinetic barriers for different geometric approaches for dimerization suggest an explanation why oligomerization stops after the formation of a dioxolane ring trimer as observed experimentally.

Introduction

The climactic effects of aerosol/cloud interactions have proven difficult to quantify and are the major remaining uncertainty in predicting the future climate of earth.[1] Recent field studies have demonstrated that tropospheric particles with diameters below 1 μm consist mainly of internally mixed sulfate and organic species,[2] with organic species reaching 50% of the particle mass under many circumstances.[3,4] The organic aerosol component strongly influences particle growth[5] and activation into cloud droplets[6] and is therefore a major contributor to uncertainty in climate change predictions.

The organic component of atmospheric aerosol is transferred to existing particles or droplets from the gas phase, creating secondary organic aerosol (SOA). Other than this fact, the formation of organic aerosol in the troposphere is not well understood. The application of new analytical methods has revealed that SOA contains significant amounts of oligomeric macromolecules formed by particle-phase reactions.[7−17] The oligomeric material, however, remains poorly characterized in terms of its sources, its structure, and its subsequent effects on the particle (and therefore climate). Although many reactions involving aldehydes have been proposed to explain these observations,[16−18] experimental evidence is limited.[15−17]

Because glyoxal is produced by the atmospheric oxidation of anthropogenic (aromatic)[10,19,20] and biogenic hydrocarbons,[21] it is present throughout the terrestrial troposphere in the low-part-per-billion range or above.[21−23] Urban field measurements indicate that glyoxal is removed from the gas phase at a rate much faster than can be accounted for by its photolysis, suggesting rapid uptake by aerosol particles.[24] These observations indicate that glyoxal may be a significant source of SOA, accounting for approximately one-sixth of the total observed SOA formation in Mexico City. Glyoxal is also scavenged by cloud droplets in the atmosphere.[25] As a result, glyoxal is one of the two most common aldehydes found in clouds, dew, and fogwater.[23,26,27] Glyoxal uptake into clouds is not entirely reversible. When a cloud droplet evaporates, a significant percentage of its glyoxal is left behind in a residual, cloud-processed aerosol particle.[28] Thus, cloud processing is a second pathway by which glyoxal could generate SOA.

Particle chamber studies have been performed without gas-phase oxidants to determine the mechanism of glyoxal uptake.[29−32] In these studies, glyoxal was taken up by aerosol particles at relative humidity levels as low as 26%.[29] This uptake was caused by the formation of low-volatility glyoxal hydrates and $n \leq 3$ oligomers.[31,32] The formation of glyoxal dihydrate (reaction 1 in Figure 1) is extremely favorable in the aqueous phase, resulting in large effective Henry's law coefficients $K^*_H = 3.6 \times 10^5$ M/atm in bulk seawater[33] and $K^*_H = 2.6 \times 10^7$ M/atm on ammonium sulfate aerosol particles at ~50% relative humidity.[30] NMR and FTIR−attenuated total reflectance (ATR) spectroscopic studies suggest that glyoxal oligomers are formed from the self-reactions of singly hydrated monomers[28] in the condensed phase via acetal linkages into dioxolane rings,[34,35] as shown in reactions 2 and 3 in Figure 1. Although these reactions are at equilibrium in solution,[34,35] drying a droplet of aqueous glyoxal solution caused the reactions to shift entirely to the product side.[28] Finally, because glyoxal oligomers are unstable below pH = 2,[36] glyoxal uptake by aerosol is enhanced only under mildly acidic conditions.[32]

Three recent theoretical studies have surveyed proposed SOA-forming reactions. The first two studies by Barsanti and Pankow[37,38] used empirical and Benson thermochemical data and applied thermodynamic principles to calculate the accretion of different SOA products. They concluded that glyoxal and methylglyoxal, but no other small carbonyl compounds, could form SOA via condensed-phase reactions at atmospheric conditions. The third study by Tong et al.[39] used density functional theory calculations to show that dimerization and trimerization thermodynamically favor forming five-membered dioxolane rings (reactions 2 and 3 in Figure 1) over six-membered dioxane rings. Reaction barriers were not calculated since they were not studying the mechanism, and the estimation of the entropic contribution differs from our present study. We complement these studies by providing kinetic data, thereby explaining some of these reactions in unprecedented mechanistic detail. Furthermore, our study provides a template to systematically characterize closely related SOA reactions from first principles. One

* Corresponding author. E-mail: jkua@sandiego.edu.

10.1021/jp076573g CCC: $40.75
Published on Web 12/08/2007

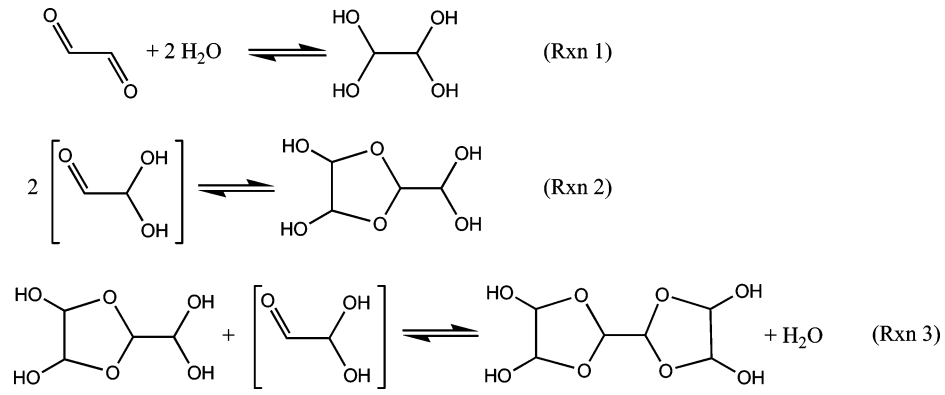

Figure 1. Reactions of glyoxal.

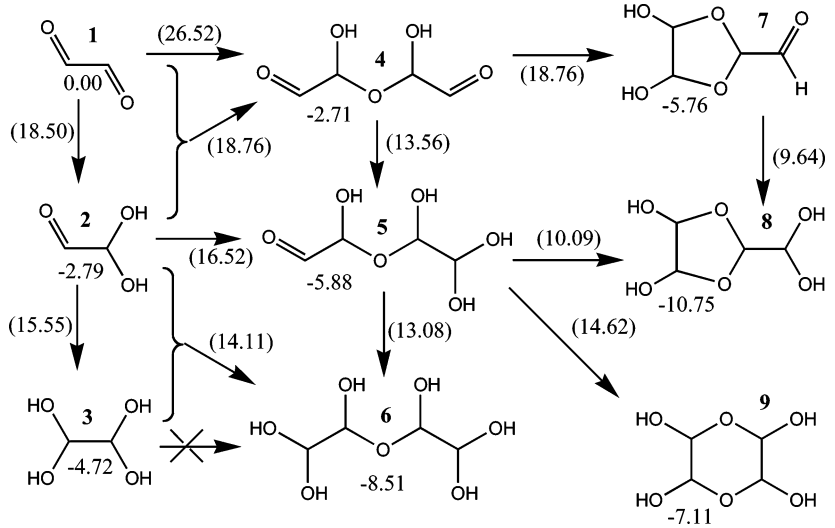

Figure 2. Monomers and dimers considered in the transformation of glyoxal in solution including *relative* free energies (in kcal/mol) for all species in solution referenced to glyoxal and water. Reactants, products, and intermediates are in bold print; transition states are in parentheses.

reason why ab initio studies have rarely been applied to SOA formation is because the chemical reactions involved and the SOA reaction matrix are both largely uncharacterized.

Our present study aims to shed light on the observed multiphase behavior of glyoxal and to suggest detailed mechanisms of oligomer formation. Although these detailed mechanisms apply only to the self-reaction of glyoxal, they can be used to identify other potential atmospheric reaction partners for glyoxal. The reactants, products, and intermediates considered in our study are shown in Figure 2. We find hydration of carbonyl groups (**1** → **2** → **3**, **4** → **5** → **6**, **7** → **8**) to be thermodynamically favorable. The kinetic barriers to hydration are higher for the monomer than the dimer. We find that oligomerization and ring closure are most favorable kinetically when an sp^3 oxygen of an OH group acts as a nucleophile attacking the carbonyl carbon; hydrogen is transferred to the carbonyl oxygen mediated by a hydrogen-bond network. Since all barriers are relatively low, it is therefore favorable for dehydration to occur prior to formation of a new C−O bond. The dioxolane ring dimer **8** is the thermodynamic sink and has the lowest barrier to formation. We find that the favored geometric approach for oligomerization suggests why the dioxolane ring trimer (reaction 3 in Figure 1) is the end point of the reaction.

The article is organized as follows. After describing the computational methods, which include validation of our free energy approximation, we will discuss the results for the three types of reactions considered: hydration, dimerization, and ring closure. We will then conclude by summarizing the overall reaction pathway, suggesting what to expect for larger oligomers, and discussing how the current study may serve as a precursor to future work. Note, in particular, that the free energies in Figure 2 are *relative* to glyoxal and water as the reference state, whereas those in Tables 2−4 are for the reactions listed in the left column of each table. Geometries of the reactants, products, intermediates, and transition states in Cartesian coordinates are provided in the Supporting Information.

Computational Methods

All calculations were carried out using Jaguar 6.0[40] at the B3LYP[41−44] flavor of density functional theory (DFT) with a 6-311G** basis set. To maximize the probability of finding the global minimum, we performed calculations on various conformers of each structure with different internal hydrogen-bond networks. Higher energy conformers are only included where relevant in the discussion. Otherwise only the lowest energy conformer results are shown in Table 1. The electronic energy of the optimized gas-phase structures is designated E_{elec}. Each of these structures was then subject to solvation, zero-point energy, and thermodynamic corrections to 298 K, as described below.

The Poisson−Boltzmann (PB) continuum approximation[45,46] was used to describe the effect of solvent. In this approximation, a smooth solvent-accessible surface of the solute is calculated by rolling a sphere of radius R_{solv} over the van der Waals surface. The solvent is represented as a polarizable continuum surround-

TABLE 1: Calculated Energies for All Species Showing Relative Contributions of Each Component

	E_{elec} (au)[a]	E_{solv} (kcal/mol)	H_{corr} (kcal/mol)	G_{corr} (kcal/mol)	$-0.5\ TS$ (kcal/mol)	G_{298} (kcal/mol)
H_2CO	−114.53629	−2.66	19.01	3.44	−7.79	−71864.1
$H_2CO{\cdot}2H_2O$	−267.46008	−11.90	54.22	28.66	−12.78	−167804.2
TS−H_2CO	−267.42805	−13.44	51.27	30.45	−10.41	−167786.2
$H_2C(OH)_2$	−191.00300	−11.57	38.81	19.98	−9.42	−119838.4
H_2O	−76.44744	−8.11	15.74	2.30	−6.72	−47970.6
1	−227.88558	−4.03	26.33	7.03	−9.65	−142987.7
2	−304.35556	−9.48	45.36	23.43	−10.97	−190961.1
3	−380.82792	−13.41	64.66	41.22	−11.72	−238933.6
4	−532.25078	−15.90	74.23	44.95	−14.64	−333948.8
5	−608.73152	−16.03	93.60	63.12	−15.24	−381922.5
6	−685.19987	−22.97	112.81	80.59	−16.11	−429895.8
7	−532.26331	−13.49	75.42	48.57	−13.43	−333951.8
8	−608.73954	−17.84	94.72	65.95	−14.39	−381927.4
9	−608.73770	−16.35	95.01	67.64	−13.69	−381923.8
H1	−380.77984	−13.79	58.43	34.32	−12.06	−238910.4
H2	−457.25453	−17.59	77.99	52.47	−12.76	−286884.0
H4	−685.15745	−21.25	107.21	73.65	−16.78	−429873.7
H5	−761.62738	−25.83	126.42	92.68	−16.87	−477844.8
H7	−685.16497	−22.85	107.90	77.76	−15.07	−429877.6
D11	−532.19944	−14.92	70.11	41.14	−14.49	−333919.6
D12	−608.67662	−18.56	86.89	55.27	−15.81	−381897.9
D22	−685.14957	−22.34	105.94	73.13	−16.41	−429870.7
D23	−761.62573	−24.72	125.41	91.46	−16.98	−477843.7
D23b	−761.62704	−21.50	125.43	92.09	−16.67	−477841.0
D23c	−761.61632	−19.13	125.69	91.50	−17.10	−477832.1
R7	−608.68921	−17.05	87.86	58.88	−14.49	−381902.0
R8	−685.16445	−22.00	107.32	76.89	−15.22	−429877.2
R9	−685.16377	−19.03	107.99	78.48	−14.76	−429872.6

[a] 1 au = 627.5096 kcal/mol.

TABLE 2: ΔG and $\Delta G^{\ddagger}$ (in kcal/mol) for Hydration Reactions

reaction	ΔG (kcal/mol)	$\Delta G^{\ddagger}$ (kcal/mol)	transition state
1 + H_2O → **2**	−2.8	18.5	**H1**
2 + H_2O → **3**	−1.9	18.3	**H2**
4 + H_2O → **5**	−3.2	16.3	**H4**
5 + H_2O → **6**	−2.6	19.0	**H5**
7 + H_2O → **8**	−5.0	15.4	**H7**

TABLE 3: ΔG and $\Delta G^{\ddagger}$ (in kcal/mol) for Dimerization Reactions

reaction	ΔG (kcal/mol)	$\Delta G^{\ddagger}$ (kcal/mol)	transition state
1 + **1** + H_2O → **4**	−2.7	26.5	**D11**
1 + **2** → **4**	+0.1	21.6	**D12**
2 + **2** → **5**	−0.3	22.1	**D22**
2 + **3** → **6**	−1.0	21.6	**D23**

TABLE 4: ΔG and $\Delta G^{\ddagger}$ (in kcal/mol) for Ring Closure Reactions

reaction	ΔG (kcal/mol)	$\Delta G^{\ddagger}$ (kcal/mol)	transition state
4 → **7**	−3.1	21.5	**R7**
5 → **8**	−4.9	16.0	**R8**
5 → **9**	−1.3	20.5	**R9**

ing the molecule with dielectric constant ϵ. Charges are allowed to develop on the surface according to the electrostatic potential of the solute and ϵ; then the polarized reaction field of the solvent acts back on the quantum mechanical description of the solute. The wave function of the complex is relaxed self-consistently with the reaction field to solve the PB equations. Although the forces on the quantum mechanical solute atoms due to the solvent can be calculated in the presence of the solvent, in this work, the solvation energy was calculated at the optimized gas-phase geometry for all structures at minima. This is because there is little change between the gas-phase and implicit solvent optimized geometries. The difference in energy between the unsolvated and solvated structures is designated E_{solv}. The parameters used for the dielectric constant and probe radius are $\epsilon = 80.4$ and $R_{solv} = 1.40$ Å for water. The solvation energy is designated E_{solv} in Table 1. It is important to note that even though the solvation energy contribution is to some extent a free energy correction, it certainly does not account for all of the free energy.

The analytical Hessian was calculated for each optimized geometry in the gas phase. The DFT gas-phase energy was then corrected for zero-point vibrations. Negative eigenvalues in transition state calculations were not included in the zero-point energy (ZPE). The temperature-dependent enthalpy correction term is straightforward to calculate from statistical mechanics. Assuming that the translational and rotational corrections are a constant times kT, that low-frequency vibrational modes will generally cancel out when calculating enthalpy differences, and that the vibrational frequencies do not change appreciably in solution, we can calculate H_{298K}. The combined ZPE and enthalpy corrections to 298 K are designated H_{corr}, and the corresponding *gas-phase* free energy correction to 298 K is designated G_{corr} in Table 1.

The corresponding free energy corrections in solution are much less reliable.[47−49] Changes in free energy terms for translation and rotation are poorly defined in solution, particularly as the size of the molecule increases. Additional corrections to the free energy for concentration differentials among species (to obtain the chemical potential) can be significant, especially if the solubility varies among the different species in solution. Furthermore, since the reactions being studied are in solution, the free energy being accounted for comes from two different sources: thermal corrections and implicit solvent. Neither of these parameters is easily separable, nor do they constitute all the required parts of the free energy under our approximations of the system.

To estimate the free energy, we followed the method of Lau and Deubel[50] who included the solvation entropy of each species

as *half* of its gas-phase entropy. Wertz[51] and Abraham[52] had previously suggested that upon dissolving in water, molecules lose a constant fraction (~0.5) of their entropy. In Table 1, this is designated $-0.5TS$ and is calculated by $0.5(G_{corr} - H_{corr})$. The free energy of each species, designated G_{298}, is the sum of E_{elec}, E_{solv}, H_{corr}, and $-0.5TS$. Our reported ΔG values are calculated from the difference in G_{298} between the reactants and products. Unless indicated otherwise, all ΔG values refer to the solution phase.

Since experimental ΔG values are unavailable for the transformation of glyoxal, we chose to test our method on the hydration of formaldehyde to form methanediol. The overall reaction is given by

$$H_2CO + H_2O \rightarrow H_2C(OH)_2$$

Early experiments[53] measured an equilibrium constant of 2×10^3 corresponding to $\Delta G = -4.5$ kcal/mol, while recent measurements[54] yield $\Delta G = -4.2$ kcal/mol. The most recent experimental measurement of ΔH for this reaction is -7.5 kcal/mol, by Winkelman et al.[54] (who also discuss prior ΔH measurements that range from -5 to -9 kcal/mol). Our calculated ΔG and ΔH values of -3.8 and -8.8 kcal/mol, respectively, are reasonably close to experimental values.

The experimentally measured barrier for this reaction $\Delta G^{\ddagger}$ is 16 kcal/mol.[54,55] To optimize the transition state, we added an additional water molecule into the system to yield a six-center transition state. In a previous study we had found that four-center transition states in condensation/hydrolysis reactions yield unrealistically high barriers.[56] Our calculated $\Delta G^{\ddagger}$ of 19.0 kcal/mol using the Wertz fraction of 0.5 for the entropy correction[51] is still 3 kcal/mol too high. If we examine the calculated energetics of forming the reactant adduct $H_2CO{\cdot}2H_2O$ from the reactants, $\Delta G = +1.0$ kcal/mol after applying the 0.5 fraction entropy correction. The final result really should be zero since adding the two water molecules into the calculation explicitly should not change ΔG. If instead a 0.6 fraction was applied (i.e., using $-0.6TS$) then indeed ΔG is zero for forming the reactant adduct. In this case, for the hydration reaction, we would calculate $\Delta G = -4.2$ kcal/mol (equal to the experimental value) and $\Delta G^{\ddagger} = 18.4$ kcal/mol which is still too high. In our calculations involving the hydration of glyoxal, we also find a similar discrepancy where ΔG between reactant and reactant·water adduct is ~1 kcal/mol rather than zero; and using $-0.6TS$ eliminates this discrepancy. Although this is true for most of our calculated reactions, a few require (e.g., some of the oligomerization reactions) a different correction; we find that the correction would range between $-0.4TS$ and $-0.6TS$. We therefore chose to maintain the standard 0.5 fraction entropy correction in all our reported results. With these approximations, we expect that our calculated ΔG values are reasonably good (within a kcal/mol), but our $\Delta G^{\ddagger}$ values will be systematically ~3 kcal/mol too high.

Results and Discussion

Hydration Reactions. Hydration reactions are represented by the vertical down arrows in Figure 2. Based on the energies in Table 1, we can calculate ΔG and $\Delta G^{\ddagger}$ for each reaction. Addition of one water molecule converts **1** to its monohydrate **2**. For this reaction $\Delta G = -2.8$ kcal/mol. If only one water molecule is included in the transition state, this results in a four-center transition state with $\Delta G^{\ddagger} = 37.0$ kcal/mol. If two water molecules are included, there is a six-center transition state **H1** with $\Delta G^{\ddagger} = 18.5$ kcal/mol. Addition of a third water molecule also resulted in a six-center transition state ($\Delta G^{\ddagger} = 18.8$ kcal/mol) with the third water molecule migrating to form a hydrogen-bond network with the other end of **1**. These three transition states are shown in Figure 3. For all subsequent hydration transition states, we added two water molecules analogous to **H1**. The transition states **H2**, **H4**, **H5**, **H7** for the hydration of **2**, **4**, **5**, **7**, respectively, are all six-center transition states similar in geometry to **H1**. The energy changes for the hydration reactions are summarized in Table 2. The structure of **H2** is also shown in Figure 3. The hydration reactions are all thermodynamically favorable with barriers ranging from 15.4 to 19.0 kcal/mol.

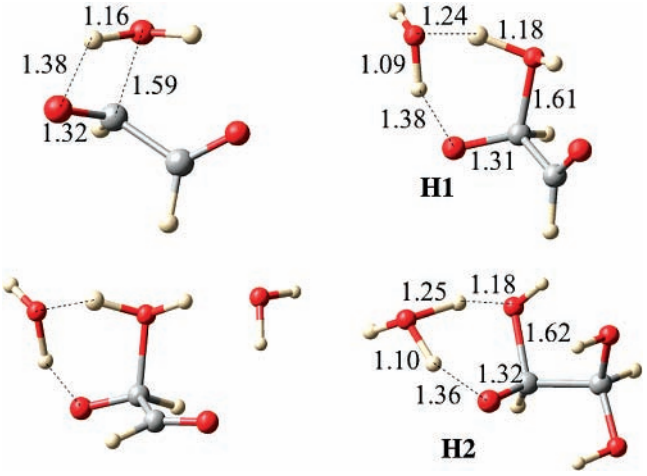

Figure 3. Transition state structures for hydration of glyoxal to form glyoxal dihydrate. The structures on the left show the first hydration reaction with one and three additional water molecules, respectively.

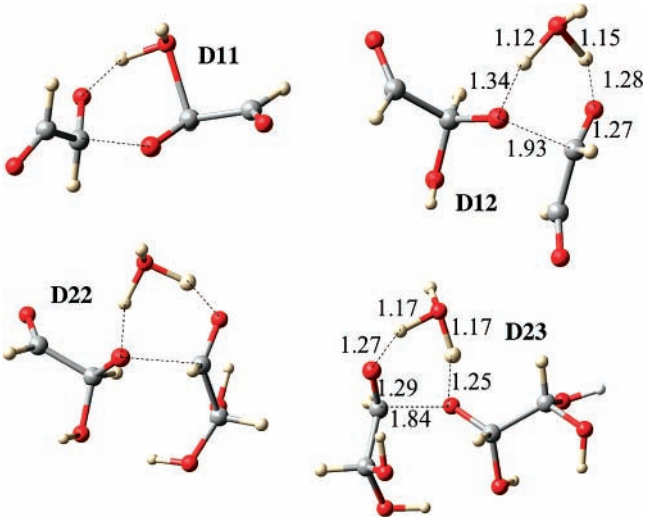

Figure 4. Transition state structures for dimerization reactions.

Dimerization Reactions. Dimerization of **1** to form **4** with an sp^2 carbonyl oxygen as the nucleophile is thermodynamically favorable ($\Delta G = -2.7$ kcal/mol) but has a high barrier ($\Delta G^{\ddagger} = 26.5$ kcal/mol). Water must be simultaneously added to the carbonyl carbon with one of its hydrogens starting to migrate to the other glyoxal molecule. The resulting six-center transition state **D11** is shown in Figure 4. If instead, **4** is formed by adding **1** and **2** with the sp^3 hydroxyl oxygen on **2** as the nucleophile, the barrier is lower ($\Delta G^{\ddagger} = 21.6$ kcal/mol). The resulting six-center transition state **D12**, with an additional water molecule, is also shown in Figure 4 and is similar to condensation reaction transition states in other systems.[56]

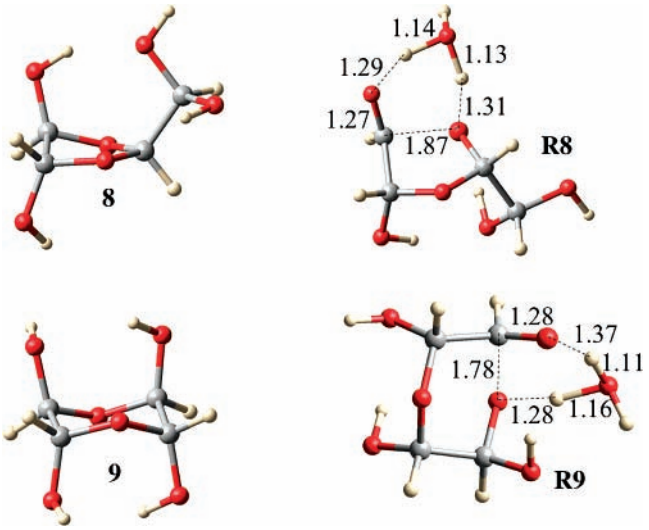

Figure 5. Structures of **8**, **9**, **R8**, **R9**.

Dimerization of **2** forms the open dimer monohydrate **5** with a similar transition state (**D22**) and barrier ($\Delta G^{\ddagger}$ = 22.1 kcal/mol) to **D12**. Since the dimerization barriers (21−22 kcal/mol) are higher than the hydration barriers (18−19 kcal/mol), and hydration of glyoxal is thermodynamically favorable, we expect that prior to dimerization the predominant monomer species is the dihydrate **3**. Attempts to dimerize **3** directly to form **6** via an S_N2 attack of an OH oxygen nucleophile to an sp^3 rather than an sp^2 carbon all resulted in high barriers ($\Delta G^{\ddagger} > 40$ kcal/mol) even with the addition of up to four additional water molecules that form hydrogen-bond networks with the incoming nucleophile and the leaving group. In fact, after substantially exploring the potential energy surface at the initial stages of attack, we found that the most favorable pathway always involved dehydration of one of the dihydrates into a monohydrate, i.e., the sp^2 carbon presents a better electrophile than the sp^3 carbon. The addition of **2** and **3** to form **6** via transition state **D23** (shown in Figure 5) has a similar structure and barrier ($\Delta G^{\ddagger}$ = 21.6 kcal/mol) to **D12** and **D22**, as expected. We therefore expect dehydration of the monomers to precede dimerization. At high monomer concentration, temporary dehydration of a monomer followed by nucleophilic attack from a neighboring monomer results in the formation of the open dimer dihydrate **6**, the dominant open dimer species. In the atmosphere, temporary dehydration of a monomer may instead be followed by an attack by a more abundant or stronger nucleophile. The dimerization reaction energies are summarized in Table 3. Note that the ΔG values are relatively close to zero for the reactions with $\Delta G^{\ddagger}$ in the 21−22 kcal/mol range.

Ring Closure. Since ring closure involves nucleophilic attack similar to dimerization, temporary dehydration of **6** into **5** is expected prior to ring formation. Two possible ring structures can be formed via intramolecular nucleophilic attack on the sp^2 carbon: the five-membered dioxolane ring dimer **8** and the six-membered dioxane ring dimer **9**. Formation of both rings from **5** is thermodynamically favorable. The lowest energy structure of **8** has the 1,2-diol group in the trans conformation (although there is a cis conformer only 0.8 kcal/mol higher in energy); there is one hydrogen bond between a ring hydroxyl and a terminal hydroxyl. The lowest energy structure of **9** has both 1,2-diol groups in the trans conformation with hydrogen bonds bridging the hydroxyl groups. Both structures are shown in Figure 5.

Ring closure to form **8** has a significantly lower barrier ($\Delta G^{\ddagger}$ = 16.0 kcal/mol) than **9** ($\Delta G^{\ddagger}$ = 20.5 kcal/mol). Formation of **8** is also thermodynamically more favorable (ΔG = −4.9 kcal/mol) than **9** (ΔG = −1.23 kcal/mol). The corresponding transition states **R8** and **R9** are also shown in Figure 5. Comparison of these values to the hydration of **5** to form **6** (ΔG = −2.6 kcal/mol and $\Delta G^{\ddagger}$ = 19.0 kcal/mol) suggests that **9** is unlikely to be observed, in agreement with experiment. The dioxolane ring **8** is the thermodynamic sink for all monomers and dimers and also has the lowest barrier to formation. Therefore, we expect that upon dimerization to form **6**, dehydration to form the intermediate **5** leads quickly and easily to ring closure, forming **8**. For completeness, we also calculated the ring closure of **4** to form **7** via transition state **R7** although we do not expect this to be an important contributor to the mechanism except at very highly concentrated glyoxal solutions where hydration reactions do not predominate. The ring closure reaction energies are summarized in Table 4.

FTIR−ATR observations of drying glyoxal solutions have provided indirect evidence that loss of hydrate water from glyoxal precedes oligomerization or ring closure.[28] In this study, IR absorbance bands near 950 cm^{-1} assigned to asymmetric stretching of C−O−C linked glyoxal dimers and trimers appeared only after the spectral signature of liquid water disappeared. Furthermore, no band due to carbonyl stretching was observed in glyoxal solutions, suggesting a nucleophilic attack follows immediately after the dehydration step **3** back to **2**. This nucleophilic attack prevents further dehydration to volatile **1**, explaining observations that glyoxal does not evaporate from concentrated solutions.

Overall Reaction Pathways. To compare the relative energies of all reactants, products, intermediates, and transition states, we chose glyoxal and water as the zero-energy reference state. The *relative* free energy of the lowest energy conformer of each species is shown in Figure 2. At very dilute concentrations of glyoxal, the dominant species is the dihydrate **3** since hydration is thermodynamically favorable and the energy barriers are relatively low. As the concentration of glyoxal increases in solution, or under dehydrating conditions, dimerization takes place via transition state **D23** to form **6**. Dehydration of **6** into **5** easily leads to ring closure via transition state **R8** into the dioxolane ring dimer **8**, the dominant dimer species. The open dimer monohydrate **5** is a key intermediate since it can potentially hydrate back into **6**, form the five-membered ring **8** or the six-membered ring **9**. All three reactions are thermodynamically favorable with the most favorable being formation of **8**, followed by **6**, then **9**. The relative barriers follow the same order. (Note that **5** could also dehydrate into **4** and then undergo ring closure to **7**, which hydrates into **8**.)

Figure 6 shows symmetric ring-containing trimers that can potentially be formed. Under dehydrating conditions, oligomerization stops at the symmetric trimer **10** formed by adding a monomer to the 1,1-diol end of **8** and subsequent ring closure. Two other trimers, **11** and **12**, can conceivably be formed by adding a monomer to the 1,2-diol ends of **8** and **9**, respectively, followed by ring closure. These latter two trimers are not observed experimentally, suggesting that the addition of a monomer to the 1,1-diol is favorable, but not to the 1,2-diol that forms part of the ring. One possible explanation is that the ring limits the conformations of the two hydroxyl groups in the 1,2-diol, because there is no longer free rotation around the C−C bond, leading to a narrow high-energy transition state. We chose to study the geometric approach of a 1,1-diol versus a 1,2-diol without constraining free rotation around the C−C bond, while at the same time limiting our calculations to only monomers and dimers. We chose not to explicitly calculate

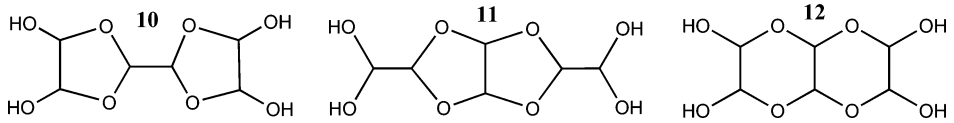

Figure 6. Potential ring closure trimer structures.

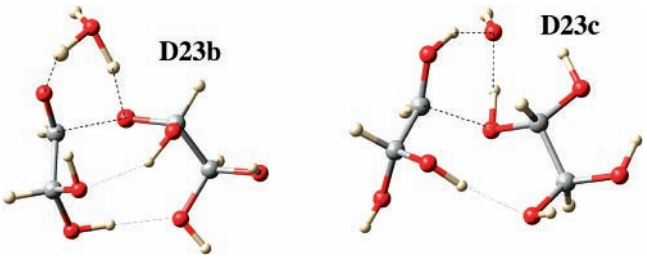

Figure 7. Transition state structures of **D23b**, **D23c**.

trimers for two reasons: (a) the detailed mechanism of dimerization should allow us to predict the pathway for higher oligomerization, and (b) we plan to run a larger scale molecular dynamics simulation with a reactive force field,[57] that makes use only of monomers and dimers and no larger oligomers in its parametrization, to study the distribution of all oligomers in solution.

The dominant dimerization reaction of glyoxal in solution goes through transition state **D23** involving the approach of the 1,1-diol with one of the hydroxyls acting as a nucleophile (see Figure 4). We tried several other geometric approaches where hydrogen bonding can be formed with the hydroxyl groups on the other end of the nucleophile. The lowest energy transition state is **D23b**, shown in Figure 7, with $\Delta G^{\ddagger} = 24.3$ kcal/mol, 2.7 kcal/mol higher than **D23**. However, this hydrogen-bonding network will not be observed for adding a monomer to either **8** or **9** because of the ring system. The best transition state structure that comes close to having an appropriate hydrogen-bond network that may be observed for a ring-constrained 1,2-diol is **D23c** (see Figure 7), which is significantly higher in energy with $\Delta G^{\ddagger} = 33.3$ kcal/mol. We think this much higher barrier is why **11** and **12** are not observed experimentally and that **10** is the endpoint of oligomerization.

Conclusion

We have applied DFT calculations to study the hydration of glyoxal and its subsequent oligomerization in solution. Relative free energies of intermediates and transition states were calculated, giving us an overall picture of the thermodynamics and kinetics of the system, allowing us to propose detailed reaction mechanisms. We find that hydrated species are thermodynamically favored over their less hydrated counterparts; however, dimerization and subsequent ring closure proceed through a preliminary dehydration step, followed by a nucleophilic attack. The hydration/dehydration barriers are relatively low allowing for temporary formation of dehydrated intermediates. The open dimer monohydrate **5** is the key intermediate to form **8**; the barrier for ring closure is also lower than the barrier for hydration. Considering monomeric and dimeric species, our calculations show that the dioxolane ring dimer **8** is the thermodynamic sink. Based on comparing the transition states **D23** and **D23c**, we suggest why oligomerization stops after the formation of the experimentally observed dioxolane ring trimer **10** over other possibilities.

Acknowledgment. This research was supported by a Camille and Henry Dreyfus Foundation Start-Up Award and an award from Research Corporation.

Supporting Information Available: Additional tables containing structural parameters. This material is available free of charge via the Internet at http://pubs.acs.org.

References and Notes

(1) IPCC, 2007: Summary for Policymakers. In *Climate Change 2007: The Physical Science Basis. Contribution of Working Group I to the Fourth Assessment Report of the Intergovernmental Panel on Climate Change*; Solomon, S., Qin, D., Manning, M., Chen, Z., Marquis, M., Averyt, K. B., Tignor, M., Miller, H. L., Eds.; Cambridge University Press: Cambridge, United Kingdom and New York, 2007.

(2) Zhang, Q.; Canagaratna, M. R.; Jayne, J. T.; Worsnop, D. R.; Jimenez, J. L. *J. Geophys. Res.* **2005**, *110*, D07S09.

(3) Zhang, Q.; Stanier, C. O.; Canagaratna, M. R.; Jayne, J. T.; Worsnop, D. R.; Pandis, S. N.; Jimenez, J. L. *Environ. Sci. Technol.* **2004**, *38*, 4797−4809.

(4) Murphy, D. M.; Cziczo, D. J.; Froyd, K. D.; Hudson, P. K.; Matthew, B. M.; Middlebrook, A. M.; Peltier, R. E.; Sullivan, A.; Thomson, D. S.; Weber, R. J. *J. Geophys. Res.* **2006**, *111*, D23S32.

(5) Wehner, B.; Petäjä, T.; Boy, M.; Engler, C.; Birmili, W.; Tuch, T.; Wiedensohler, A.; Kulmala, M. *Geophys. Res. Lett.* **2005**, *32*, L171810.

(6) Charlson, R. J.; Seinfeld, J. H.; Nenes, A.; Kulmala, M.; Laaksonen, A.; Facchini, M. C. *Science* **2001**, *292*, 2025−2026.

(7) Gao, S.; Ng, N. L.; Keywood, M.; Varutbangkul, V.; Bahreini, R.; Nenes, A.; He, J.; Yoo, K. Y.; Beauchamp, J. L.; Hodyss, R. P.; Flagan, R. C.; Seinfeld, J. H. *Environ. Sci. Technol.* **2004**, *38*, 6582−6589.

(8) Iinuma, Y.; Boege, O.; Gnauk, T.; Herrmann, H. *Atmos. Environ.* **2004**, *38*, 761−773.

(9) Baltensperger, U.; Kalberer, M.; Dommen, J.; Paulsen, D.; Alfarra, M. R.; Coe, H.; Fisseha, R.; Gascho, A.; Gysel, M.; Nyeki, S.; Sax, M.; Steinbacher, M.; Prevot, A. S. H.; Sjoegren, S.; Weingartner, E.; Zenobi, R. *Faraday Discuss.* **2005**, *130*, 265−278.

(10) Paulson, D.; Dommen, J.; Kalberer, M.; Prévôt, A. S. H.; Richter, R.; Sax, M.; Steinbacher, M.; Weingartner, E.; Baltensperger, U. *Environ. Sci. Technol.* **2005**, *39*, 2668−2678.

(11) Angove, D. E.; Fookes, C. J. R.; Hynes, R. G.; Walters, C. K.; Azzi, M. *Atmos. Environ.* **2006**, *40*, 4597−4607.

(12) Dommen, J.; Metzger, A.; Duplissy, J.; Kalberer, M.; Alfarra, M. R.; Gascho, A.; Weingartner, E.; Prévôt, A. S. H.; Verheggen, B.; Baltensperger, U. *Geophys. Res. Lett.* **2006**, *33*, L13805.

(13) Paulson, D.; Weingartner, E.; Alfarra, M. R.; Baltensperger, U. *J. Aerosol Sci.* **2006**, *37*, 1025−1051.

(14) Hearn, J. D.; Smith, G. D. *Int. J. Mass Spectrom.* **2006**, *258*, 95−103.

(15) Kalberer, M.; Paulsen, D.; Sax, M.; Steinbacher, M.; Dommen, J.; Prevot, A. S. H.; Fisseha, R.; Weingartner, E.; Frankevich, V.; Zenobi, R.; Baltensperger, U. *Science* **2004**, *303*, 1659−1662.

(16) Tolocka, M. P.; Jang, M.; Ginter, J. M.; Cox, F. J.; Kamens, R. M.; Johnston, M. V. *Environ. Sci. Technol.* **2004**, *38*, 1428−1434.

(17) Gao, S.; Keywood, M.; Ng, N. L.; Surratt, J.; Varutbangkul, V.; Bahreini, R.; Flagan, R. C.; Seinfeld, J. H. *J. Phys. Chem. A* **2004**, *108*, 10147−10164.

(18) Jang, M.; Czoschke, N. M.; Lee, S.; Kamens, R. M. *Science* **2002**, *298*, 814−817.

(19) Andino, J. M.; Smith, J. N.; Flagan, R. C.; Goddard, W. A., III; Seinfeld, J. H. *J. Phys. Chem.* **1996**, *100*, 10967−10980.

(20) Volkamer, R.; Platt, U.; Wirtz, K. *J. Phys. Chem. A* **2001**, *105*, 7865−7874.

(21) Volkamer, R.; Barnes, I.; Platt, U.; Molina, L. T.; Molina, M. J. Remote sensing of glyoxal by differential optical absorption spectroscopy (DOAS): advances in simulation chamber and field experiments. In *Proceedings of the NATO Advanced Research Workshop "Environmental Simulation Chambers: Application to Atmospheric Chemical Processes"*; Ruczinski, K., Barnes, I., Eds.; NATO Sciences Series: Zakopane, Poland, 2004; Vol. IV. Copy available upon e-mail request from rainer@alum.mit.edu.

(22) Grossmann, D.; Moortgat, G. K.; Kibler, M.; Schlomski, S.; Schmann, K. B.; Alicke, B.; Geyer, A.; Platt, U.; Hammer, M.-U.; Vogel, B.; Mihelcic, D.; Hofzumahaus, A.; Holland, F.; Volz-Thomas, A. *J. Geophys. Res.* **2003**, *108*, 8250−8269.

(23) Matsumoto, K.; Kawai, S.; Igawa, M. *Atmos. Environ.* **2005**, *39*, 7321−7329.

(24) Volkamer, R.; San Martini, F.; Molina, L. T.; Salcedo, D.; Jimenez, J. L.; Molina, M. J. *Geophys. Res. Lett.* **2007**, *34*, L19807.

(25) Schweitzer, F.; Magi, L.; Mirabel, P.; George, C. *J. Phys. Chem. A* **1998**, *102*, 593−600.
(26) Igawa, M.; Munger, J. W.; Hoffmann, M. R. *Environ. Sci. Technol.* **1989**, *23*, 556−561.
(27) Munger, J. W.; Jacob, D. J.; Daube, B. C.; Horowitz, L. W.; Keene, W. C.; Heikes, B. G. *J. Geophys. Res.* **1995**, *100*, 9325−9333.
(28) Loeffler, K. W.; Koehler, C. A.; Paul, N. M.; De Haan, D. O. *Environ. Sci. Technol.* **2006**, *40*, 6318−6323.
(29) Hastings, W. P.; Koehler, C. A.; Bailey, E. L.; De Haan, D. O. *Environ. Sci. Technol.* **2005**, *39*, 8728−8735.
(30) Kroll, J. H.; Ng, N. L.; Murphy, S. M.; Varutbangkul, V.; Flagan, R. C.; Seinfeld, J. H. *J. Geophys. Res.* **2005**, *110*, D23207.
(31) Liggio, J.; Li, S.-M.; McLaren, R. *Environ. Sci. Technol.* **2005**, *39*, 1532−1541.
(32) Liggio, J.; Li, S.-M.; McLaren, R. *J. Geophys. Res.* **2005**, *110*, D10304.
(33) Zhou, X.; Mopper, K. *Environ. Sci. Technol.* **1990**, *24*, 1864−1869.
(34) Chastrette, F.; Bracoud, C.; Chastrette, M.; Mattioda, G.; Christidis, Y. *Bull. Soc. Chim. Fr.* **1983**, II-33−II-40.
(35) Chastrette, F.; Chastrette, M.; Bracoud, C. *Bull. Soc. Chim. Fr.* **1986**, 822−836.
(36) Fratzke, A. R.; Reilly, P. J. *J. Chem. Kinet.* **1986**, *18*, 775.
(37) Barsanti, K. C.; Pankow, J. F. *Atmos. Environ.* **2004**, *38*, 4371−4382.
(38) Barsanti, K. C.; Pankow, J. F. *Atmos. Environ.* **2005**, *39*, 6597−6607.
(39) Tong, C.; Blanco, M.; Goddard, W. A., III; Seinfeld, J. H. *Environ. Sci. Technol.* **2006**, *40*, 2333−2338.
(40) *Jaguar v6.0*; Schrodinger, LLC: Portland, OR, 2005.
(41) Becke, A. D. *J. Chem. Phys.* **1993**, *98*, 5648.
(42) Becke, A. D. *Phys. Rev. A* **1988**, *38*, 3098.
(43) Vosko, S. H.; Wilk, L.; Nusair, M. *Can. J. Phys.* **1980**, *58*, 1200.
(44) Lee, C.; Yang, W.; Parr, R. G. *Phys. Rev. B* **1988**, *37*, 785.
(45) Tannor, D. J.; Marten, B.; Murphy. R.; Friesner, R. A.; Sitkoff, D.; Nicholls, A.; Ringnalda, M.; Goddard, W. A., III; Honig, B. *J. Am. Chem. Soc.* **1994**, *116*, 11875.
(46) Marten, B.; Kim, K.; Cortis, C.; Friesner, R. A.; Murphy, R. B.; Ringnalda, M. N.; Sitkoff, D.; Honig, B. *J. Phys. Chem.* **1996**, *100*, 11775.
(47) Wiberg, K. B.; Bailey, W. F. *J. Am. Chem. Soc.* **2001**, *123*, 8231.
(48) Nielsen, R. J.; Keith, J. M.; Stoltz, B. M.; Goddard, W. A., III. *J. Am. Chem. Soc.* **2004**, *126*, 7967.
(49) Florian, J.; Warshel, A. *J. Phys. Chem. B* **1998**, *102*, 719.
(50) Lau, J. K.-C.; Deubel, D. V. *J. Chem. Theory Comput.* **2006**, *2*, 103.
(51) Wertz, D. H. *J. Am. Chem. Soc.* **1980**, *102*, 5316.
(52) Abraham, M. H. *J. Am. Chem. Soc.* **1981**, *103*, 6742.
(53) Bell, R. P. *Adv. Phys. Org. Chem.* **1966**, *4*, 1.
(54) Winkelman, J. G. M.; Voorwinde, O. K.; Ottens, M.; Beenackers, A. A. C. M.; Jannsen, L. P. B. M. *Chem. Eng. Sci.* **2002**, *57*, 4067.
(55) Guthrie, J. P. *J. Am. Chem. Soc.* **2000**, *122*, 5529.
(56) Kua, J.; Gyselbrecht, C. R. *J. Phys. Chem. A* **2007**, *111*, 4759.
(57) van Duin, A. C. T.; Dasgupta, S.; Lorant, F.; Goddard, W. A., III. *J. Phys. Chem. A* **2001**, *105*, 9396.